Line-field confocal optical coherence tomography of actinic keratosis: a case series

DR ELISA CINOTTI (Orcid ID : 0000-0002-4009-0659)

DR ARIANNA LAMBERTI (Orcid ID : 0000-0002-2291-2508)

DR JAVIERA PÉREZ ANKER (Orcid ID : 0000-0002-6959-7250)

DR MARIANO SUPPA (Orcid ID : 0000-0002-9266-0342)

Article type : Original Article

Line-field confocal optical coherence tomography for actinic keratosis and squamous cell carcinoma: a descriptive study

E. Cinotti,[1] L. Tognetti,[1] A. Cartocci,[2] A. Lamberti,[1] S. Gherbassi,[1] C. Orte Cano,[3] C. Lenoir,[3] G. Dejonckheere,[3] G. Diet,[3] M. Fontaine,[3] M. Miyamoto,[3] J. Perez-Anker,[4,5] V. Solmi,[1] J. Malvehy,[4,5] V. del Marmol,[3] J.L. Perrot,[6] P. Rubegni[1] and M. Suppa[3,7]

[1]Dermatology Unit, Department of Medical, Surgical and Neurological Sciences, University of Siena, Siena, Italy

[2]Department of Medical Biotechnologies, University of Siena, Siena, 53100, Italy.

[3]Department of Dermatology, Hôpital Erasme, Université Libre de Bruxelles, Brussels, Belgium

[4]Melanoma Unit, Hospital Clinic Barcelona, University of Barcelona, Barcelona, Spain

[5]CIBER de enfermedades raras, Instituto de Salud Carlos III, Barcelona, Spain

[6]Department of Dermatology, University Hospital of Saint-Etienne, Saint-Etienne, France

This article has been accepted for publication and undergone full peer review but has not been through the copyediting, typesetting, pagination and proofreading process, which may lead to differences between this version and the Version of Record. Please cite this article as doi: 10.1111/CED.14801

[7]Department of Dermatology, Institut Jules Bordet, Université Libre de Bruxelles, Brussels, Belgium

Correspondence: Elisa Cinotti

Email: elisacinotti@gmail.com

Conflict of Interest: None declared

Financial Support: None

Running head: LC-OCT for keratinocyte skin tumors

What's already known about this topic?

Line-field confocal optical coherence tomography (LC-OCT) is a new non-invasive imaging technique that can characterize healthy skin and basal cell carcinoma in vivo thanks to its good resolution and penetration depth. There are to date no large study on its use for the diagnosis of squamous cell carcinoma and actinic keratosis.

What does this study add?

LC-OCT can identify cellular and architectural atypia in cutaneous keratinocyte tumours and it could be useful for the differentiation of actinic keratosis from squamous cell carcinoma.

ABSTRACT

Background. Early and accurate diagnosis of cutaneous squamous cell carcinoma (SCC) and actinic keratosis (AK) is fundamental to reduce their morbidity and to select the correct treatment. Line-field confocal optical coherence tomography (LC-OCT) is a new imaging device that can characterize healthy skin and basal cell carcinoma, but no large studies are available on keratinocyte cell tumours.

Objectives. To identify and describe LC-OCT criteria associated with SCC and AK and to compare LC-OCT findings in these tumours.

Methods. A retrospective observational multicenter study was conducted. Lesions were imaged with LC-OCT device before surgery and had histological examinations. LC-OCT criteria for AK/SCC were identified and their presence was evaluated in all study lesions. Univariate and multivariate analyses were performed to compare AKs and SCCs and to investigate differences between in situ and invasive tumours.

Results. We included 158 patients with 50 AKs and 108 SCCs (62 in situ and 46 invasive). Cytological and architectural alterations were found in most lesions and differences were found among AKs and SCCs. Although the visualization of the DEJ was often hampered by hyperkeratosis and acanthosis, an outlined DEJ without broad strands was observed in almost all AKs and SCCs in situ and only in three invasive SCC ($p<0.001$) when the DEJ was detectable.

Conclusions. Our results suggest that LC-OCT can help clinicians in the identification of AK and SCC and their differentiation, providing a real-time and non-invasive examination. Further studies are needed to confirm our data.

INTRODUCTION

Cutaneous squamous cell carcinoma (SCC) is the second most frequent cancer in humans. While it usually exhibits benign clinical behaviour, it can be both locally invasive with high morbidity or metastatic with high mortality.[1,2] Actinic keratoses (AKs) are precancerous lesions that can progress into SCC.[3,4] They represent an important issue in dermatological practice because their prevalence is rising as a result of the increasing life expectancy and prolonged sun exposure.[5,6] . Bowen's disease is an intraepidermal SCC with peculiar pathogenesis and clinicopathological features, that rarely progress to invasive SCC and shows histological similarities to bowenoid AK grade III according to the classification of Röwert-Huber[7,8]. Early and accurate diagnosis of AK and SCC and identification of SCC invasiveness is relevant for the choice of the correct treatment: notably, AK can be treated with non-invasive treatments, whereas invasive SCC needs surgical excision.[9–11]

Although histological examination remains the gold standard for the diagnosis, there is an increasing interest in non-invasive imaging technologies in this field, both for the diagnosis and follow-up after non-invasive treatments.[4] Indeed, since AKs are often multiple in a field of cancerization, multiple biopsies would be needed but they would be deleterious in terms of time, cost, and aesthetic outcome.[12] Besides, non-invasive skin imaging could also guide the biopsies.

Dermoscopy is currently used in clinical practice to help the correct classification of keratinocyte skin tumours.[13–16] However, correct classification based only on clinical and dermoscopic data can be challenging and large studies on clinical and dermoscopy diagnostic accuracy for the differentiation of AK and SCC are lacking. Moreover, this technique cannot recognize subclinical AKs in the context of a field of cancerization.

Additional non-invasive tools such as reflectance confocal microscopy (RCM), conventional optical coherence tomography (OCT), and high-definition OCT (HD-OCT) provide information that is closer to the histological examination and have been investigated in terms of diagnostic performance for both clinical and subclinical keratinocyte skin tumours.[4,12] Dedicated Cochrane reviews found insufficient evidence for the use of RCM or OCT for the diagnosis of SCC.[17–19] OCT can show the destruction of

the epidermal/dermal layering in keratinocyte skin tumours but has not a sufficient resolution to identify single keratinocytes and clearly identify a keratinocyte tumour proliferation.[20] Although RCM has a higher lateral resolution than conventional OCT (1 µm vs 7.5 µm) and can detect cellular changes,[16,21] it has a lower penetration (~200 µm vs 1-2 mm) that can prevent visualization of the dermal-epidermal junction (DEJ) in hyperkeratotic lesions; besides, RCM only provides horizontal skin sections by which it is much harder to define tumour invasiveness and discriminate AK from SCC than with conventional OCT.[12,20] HD-OCT seemed to overcome the problems of both techniques by providing images with cellular resolution (isotropic resolution 3 µm), good penetration (~570 µm), and vertical sections.[22–25] Despite this device was found promising for the diagnosis of cutaneous carcinomas including AK and SCC,[22,23] its lack of handling led to its withdrawal from the market.

Recently, a new technology has been developed, named line-field confocal OCT (LC-OCT), which has far superior technical characteristics compared to HD-OCT, having a higher cell resolution (similar to RCM, just above 1 µm) with an analogue penetration depth (~500 µm).[26] Moreover, it is lighter and easier to handle and has user-friendly software. Therefore, we could expect higher diagnostic accuracy for AK and SCC and easier use in clinical practice as compared to previous OCT technologies. Recent studies have shown that LC-OCT can clearly identify different skin structures including single epidermal cells and the DEJ in healthy skin.[27] Moreover, it can reveal the cleavage level in autoimmune bullous disorders,[28] and it could aid the diagnosis of basal cell carcinoma (BCC),[29] melanocytic tumours,[30,31] vascular tumours,[32] skin infections,[33,34] genetic disorders,[35,36] and the diseases characterized by an altered keratinization.[37]

LC-OCT seems to be promising for the identification of keratinocyte tumors and their invasiveness,[12] but no large studies are available for AK and SCC. Our study aims to describe which features can be observed in AK and SCC using LC-OCT and to investigate any possible differences between these two entities.

MATERIALS AND METHODS

Study lesions

SCCs and AKs were collected from the databases of the Dermatology Departments of the Erasme University Hospital of Brussels (Belgium) and the University Hospital of Siena (Italy). The time frame of the inclusion ranged from the 1st August 2018 in Brussels and from the 1st of February 2020 in Siena, up to the 30th September 2020 for both. All lesions were excised and histopathologically-confirmed.

The study was conducted in accordance with the ethical principles of the Helsinki Declaration.

LC-OCT device

Images/videos were acquired with a CE-marked prototype of LC-OCT (DAMAE Medical, Paris, France) by two investigators expert in skin imaging (EC and MS). The device is composed of a handheld probe connected to a central unit and a display. LC-OCT is a time-domain OCT technology that uses line illumination of the skin and line detection of the signal rather than point scanning/detection. The device has 1.1-µm axial resolution, 1.3-µm lateral resolution, 500-µm scanning depth, 1.2-mm lateral field of view, and 10-frames/second acquisition.[26] Here, an LC-OCT device producing B-scans (vertically-orientated sectional images and videos) was employed.

Image acquisition protocol

A drop of paraffin oil was placed between the lesion and the glass window at the tip of the LC-OCT camera to ensure refractive index matching. Live images were directly visualized on the screen, while the operator gently moved the tip of the probe over the lesion. At least 4 LC-OCT images and 2 videos were saved for each lesion.

Image evaluation

LC-OCT criteria were chosen based on previously described histological, RCM, conventional OCT, and HD-OCT criteria for AK and SCC[20–23] and the expert opinion of the authors (**Table 1**). Three observers blinded for any clinical, dermoscopic, and histopathological data (EC, LT, and AL) retrospectively evaluated all study lesions for LC-OCT image quality (good or poor based on the visibility of the cells and the different skin

layers) and the presence/absence of each LC-OCT criterion. The thicknesses were measured using the ruler provided by the machine software. Any disagreement was solved by consensus among the evaluators.

Statistical analysis

We calculated the frequencies of qualitative variables and mean and standard deviations for quantitative variables. The association between qualitative variables and the outcome was evaluated by Fisher exact test for a 2x2 contingency table or the chi-squared for the other cases. T-test or ANOVA (respectively for AK/SCC outcome or AK/SCC in situ /SCC invasive or Bowen's disease/SCC in situ other than Bowen's disease) were carried out if the variables were normally distributed (normal distribution evaluated by Kolmogorov-Smirnov test) and there was homoscedasticity between variances evaluated by Bartlett test, otherwise Mann-Whitney or Kruskall-Wallis test was used.

Logistic regression was later performed to evaluate variables that were statistically significant at the previous univariate analysis. The best subset of variables was selected by a stepwise procedure based on Akaike's criterion. Odds ratios (ORs) and 95% confidence intervals (CIs) were estimated by logistic regression. All statistical tests were two-tailed and were considered significant for p-values <0.05. The analyses were carried out by R software version 3.6.2.

Results

Clinical features

Overall, 158 histopathologically-proven tumours (50 AKs and 108 SCCs) were included in the study (**Table 2**). Of the 108 SCCs, 62 were in situ and 46 were invasive; among the in situ group, 25 were Bowen's diseases. No bowenoid AK grade III according to Röwert-Huber[8] was included. Study lesions belonged to 83 females and 75 males; median age was 69.8±12.7 years (interval: 34–95 years); 88.0% of patients attended the Erasme University Hospital of Brussels (Belgium) and 12.0% attended the University Hospital of Siena (Italy).

The majority of SCCs were located on the head/neck region (54.6%), followed by lower extremities (17.6%), upper extremities (14.8%), and trunk (13.0%). Similarly, AKs were mainly located on the head/neck region (62.0%), followed by lower extremities (14.0%), upper extremities (12.0%), and trunk (12.0%). No statistically significant differences in gender, age, and body locations were found between AK and SCC.

LC-OCT features in univariate analysis

LC-OCT images were considered of good quality in 76.0% of AKs and 73.1% of SCCs (**Table 3**). Comparison of Bowen's disease and in situ SCC other than Bowen's disease could not find any differences, except for dyskeratotic keratinocytes that were less frequently found in Bowen's disease ($p=0.04$, marginally significant value). Therefore, Bowen's disease was pooled with SCC in situ for the comparison with AK and invasive SCC to improve the statistical power of the analyses.

The epidermis was well visible in most of the cases (95.9% of AKs and 88.8% of SCCs). Minimum, maximum, and mean lesion thickness without the stratum corneum were higher in SCC than in AK ($p<0.001$ for all) as well as the mean thickness of the stratum corneum ($p=0.02$). Hyperkeratosis was more frequent in SCC than in AK ($p=0.02$), whereas parakeratosis, erosion/ulceration and acanthosis were similarly distributed across the two entities.

Most tumours (84.0% of AKs and 91.7% of SCCs) had at least one criterion among disarranged epidermal architecture, dyskeratotic keratinocytes, and atypical nuclei. The epidermal architecture was more frequently disarranged in SCC (94.0%) than AK (77.8%, $p=0.01$). Dyskeratotic keratinocytes were appreciated in most AKs (82.2%) and SCCs (72.3%). Nuclei of keratinocytes were visible in almost all cases (96.0% of AKs and 95.3% of SCCs) and nuclei were atypical in most cases (87.2% of AKs and 91.3% of SCCs). Crowded nuclei were observed in about half of the cases (50.0% of AKs and of 47.0% SCCs).

Keratin pearls were not observed, whereas a whorled appearance of the epidermis was noticed in only 2 in situ SCCs. Mottled pigmentation of the keratinocytes and hyperpigmentation of the basal layer of the epidermis were never observed.

The DEJ was not always well visible: in 18.0% AKs and 25.0% SCCs the images did not contain the DEJ, whereas in 34.0% AKs and 34.3% SCCs it was not well defined. Outlined DEJ was consistent with histopathology in most cases and allow the distinction of AK and in situ SCC from invasive SCC. Adnexal involvement was observed in 47.7% of AKs and 36.5% of SCCs. Tumour budding was visible in about a half of AKs and SCCs, whereas broad strands were more present in invasive SCC (63.9%) than AK (3.2%) and in situ SCC (9.7%) ($p<0.001$). Dilated vessels, either glomerular or linear were found in most cases; dilated linear vessels were more frequent in AK (77.8%) than SCC (56.4%; $p=0.02$). Elastosis was observed in a small portion of cases (26.2% of AK and 12.3% of SCC).

LC-OCT features at multivariate analysis

The final logistic regression model obtained by the analysis of the LC-OCT variables that were statistically significant at the univariate analysis showed that disarranged epithelial architecture (OR 5.24, 95% CI 1.13-24.39; $p=0.035$), maximum visible lesion thickness (OR 1.02 for every µm of increased thickness, 95% CI 1.01-1.03; $p<0.001$) and broad strands (OR=8.6, 95% CI 1.49-164.63; $p=0.04$) were indicative of SCC.

DISCUSSION

Our study described LC-OCT features of keratinocyte tumours and showed that LC-OCT is able to identify major features of AK and SCC that can help their distinction. Discrimination with normal skin seems to be feasible since hyperkeratosis, acanthosis, parakeratosis, erosion/ulceration, disarranged epithelial architecture, dyskeratotic keratinocytes, crowded nuclei, atypical nuclei, tumour budding, and dilated vessels were prominent features of both AKs and SCCs. Moreover, non-outlined DEJ and broad strands characterized invasive tumours. Additional features were also revealed by the device such as the involvement of the epithelium of the hair follicle and solar elastosis. Notably, at least one among the three criteria “disarranged epithelial architecture”, “dyskeratotic keratinocytes” and “atypical nuclei” was present in most lesions; therefore,

these represented major criteria characterizing AK and SCC under LC-OCT. The disarranged epithelial architecture reflects a loss of orderly keratinocyte maturation and dyskeratotic keratinocytes indicate an altered keratinization process. Nuclei of keratinocytes are well demarcated hypo-reflective oval areas under LC-OCT and their irregularity in shape and size scored as “atypical nuclei” can be considered as an indirect sign of keratinocyte pleomorphism when using the LC-OCT device employed in this study (two-dimensional, imaging in the vertical plane). A more direct evaluation of the keratinocyte pleomorphism can be obtained with more recent and advanced LC-OCT devices, able to assess the skin in a tridimensional fashion (imaging in both the vertical and horizontal plane, tridimensional skin reconstructions).

Interestingly, LC-OCT could provide images of good quality in three-quarters of the cases despite the presence of a thick stratum corneum with a possible alteration of the imaging signal. It should be highlighted that in our study the lesions were not selected and images of all types of tumours, including clinically hyperkeratotic ones were included. Hyperkeratosis determines an excessive hyper-reflectivity of the upper part of the lesions and reduces the LC-OCT image quality of the underlying layers of the skin as it is for RCM.[38] In the future, it could be interesting to image hyperkeratotic lesions with previous application of a keratolytic cream or superficial curettage. Hyperkeratosis and acanthosis limited the visualization of the DEJ, especially in SCC, where it was not possible to reach the DEJ in one-fourth of the cases.

As compared to AK, SCC showed significantly higher mean thickness both for the lesion ($p<0.001$) and the stratum corneum ($p=0.02$), as well as more frequent disarranged epidermal architecture ($p=0.01$). Interestingly, differences between AK and SCC in minimum, maximum and mean lesion thickness, hyperkeratosis, and disarranged epidermal architecture were independent of the in situ and invasive subtype of SCC, whereas the mean thickness of the stratum corneum was higher in invasive SCC than AK. Multivariate analysis confirmed that the probability of SCC significantly increased by 2% for each µm of increment in the lesion thickness.

A non-outlined DEJ has been described as a highly accurate morphological OCT feature to distinguish SCC from AK and appeared to be related to irregular broad strands of the epidermis protruding into the upper dermis and/or presence of periadnexal collars

penetrating through the DEJ.[22] In our series, the DEJ was either not present in the image or not well visible in about half of the cases, probably due to hyperkeratosis and acanthosis. The device can scan up to a depth of 500 µm, but the image definition degrades going deep and hyperkeratosis increases the noise. Despite these limitations, when the DEJ was well detectable, it was outlined in all but two in situ lesions and only in a three invasive SCCs. Despite the small numbers (probably justifying the large CI found in our multivariate analysis), broad strands were highly suggestive of SCC; when observed in AK, they probably corresponded to hair follicles or AK PRO III[39] that could be challenging to distinguish from invasive SCC. The misclassification of hair follicles can be probably overcome in the clinical practice thanks to the real-time acquisition that allows distinguishing tumor strands from hair follicles due to their hyperreflective hair shaft moving gently the camera. The correct definition of the DEJ outline enabled us to distinguish AK and in situ SCC from invasive tumors. It should be noticed that, although the parameter "outlined DEJ" was not evaluated in some SCCs because the DEJ was not sufficiently visible, its altered visibility could be an intrinsic characteristic of the SCC and could characterize the non-outlined DEJ. Therefore, it would be interesting in future studies to better define the "non-outlined DEJ" and to include among the evaluated criteria the "interface lichenoid-like feature" appearing as an undefined hypo-reflective area obscuring DEJ. Moreover, it could be noteworthy to compare lesion thickness measured by LC-OCT and histopathology and to compare LC-OCT data with those obtained by other non-invasive imaging techniques such as RCM.

Some features such as linear dilated vessels and elastosis had unexpected higher frequencies in AK than in SCC. However, prominent vessels and elastosis have been reported in AKs in previous HD-OCT studies[40] and probably they were less visible in SCC due to thicker epidermis that prevented the dermis visualisation.

This study was performed analysing vertical sections that are quicker to evaluate and more relevant for the identification of the DEJ. However, new LC-OCT devices can acquire also horizontal sections and 3D images with a possible reconstruction through dedicated software. As already stated, better results might be obtained from the analysis of the horizontal sections, where keratinocytes have better-defined contours than in the vertical images and cell atypia can be better observed. 3D image would also enable to

clearly distinguish broad strands from hair follicles, a limitation previously mentioned with single-slice images. This could be further enhanced by the availability of real-time dermoscopic/LC-OCT correlations offered by new-generation devices that came recently on the market.

Concerning Bowen's diseases, the LC-OCT features evaluated in our study did not allow a distinction with other SCCs in situ, and further studies could be conducted to evaluate additional cytological and architectural features that could help their distinction.

Moreover, since bowenoid AK grade III according to Röwert-Huber also shows great histologic similarities to Bowen's disease, further studies could be conducted on this subtype of AKs that were absent in our series.

Our results on LC-OCT diagnosis of AKs and SCCs are encouraging and showed that higher lesion thickness, disarranged epidermal architecture and not outlined DEJ could help the differentiation of SCC from AK. Nevertheless, some limitations exist and include the retrospective design, the non-inclusion of clinical and dermoscopic features, the lack of investigation of AK grading, and the absence of comparison with other skin tumours. Tumour lobules with a triad of colour (previously described as the major LC-OCT criteria for BCC)[27] were never observed in our series and their absence favours the differential diagnosis between AK/SCC and BCC, although a comparison group was absent in the present study. Indeed, our results showed that – differently from BCC – the SCC expansion towards the dermis is characterized by tumour budding and broad strands. Moreover, AK number here was limited compared to SCCs because our study was designed to evaluate only lesions with histological examination, and lesions clinically suggestive of AK are less frequently biopsied than SCC. Finally, the LC-OCT poor image quality in one-fourth of the study cases could be regarded as another limitation; however, this was mainly related to hyperkeratosis which represents a well-known limitation for all other non-invasive imaging techniques as well, including RCM[38]. In order to report real-life data, we decided to execute this study on all lesions comprised in our databases, including the hyperkeratotic ones.

In conclusion, LC-OCT is a new non-invasive imaging technique that combines cellular resolution and visualization up to the superficial reticular dermis. It seems to be a promising tool that could help clinicians to detect cellular and architectural alterations of keratinocyte skin tumours in real-time. To our knowledge, this was the first study

describing the LC-OCT characteristics of AKs and SCCs. Our study showed that LC-OCT can identify many morphologic features such as acanthosis, hyperkeratosis, parakeratosis, erosion/ulceration, disarranged epidermal architecture, dyskeratotic keratinocytes, atypical nuclei, adnexal involvement, tumour budding, broad strands, dilated vessels, and elastosis which could be potentially useful for the diagnosis of these tumours as well as for the follow-up of non-invasive treatments. Moreover, higher lesion thickness and the presence of not outlined DEJ could help the differentiation of SCC from AK. Further studies are needed to confirm our data.

ACKNOWLEDGEMENTS

The authors are indebted to Maxime Cazalas and Clara Tavernier (DAMAE Medical, Paris, France) for their technical assistance with the LC-OCT device.

REFERENCES

1 Eigentler TK, Leiter U, Häfner H-M, *et al.* Survival of Patients with Cutaneous Squamous Cell Carcinoma: Results of a Prospective Cohort Study. *J Invest Dermatol* 2017; **137**:2309–15.

2 Burton KA, Ashack KA, Khachemoune A. Cutaneous Squamous Cell Carcinoma: A Review of High-Risk and Metastatic Disease. *Am J Clin Dermatol* 2016; **17**:491–508.

3 Fuchs A, Marmur E. The kinetics of skin cancer: progression of actinic keratosis to squamous cell carcinoma. *Dermatol Surg Off Publ Am Soc Dermatol Surg Al* 2007; **33**:1099–101.

4 Fernandez Figueras MT. From actinic keratosis to squamous cell carcinoma: pathophysiology revisited. *J Eur Acad Dermatol Venereol JEADV* 2017; **31 Suppl 2**:5–7.

5 Neidecker MV, Davis-Ajami ML, Balkrishnan R, Feldman SR. Pharmacoeconomic considerations in treating actinic keratosis. *PharmacoEconomics* 2009; **27**:451–64.

6 Cinotti E, Perrot JL, Labeille B, *et al.* Prevalence of actinic keratosis in a French cohort of elderly people: the PROOF study. *G Ital Dermatol E Venereol Organo Uff Soc Ital Dermatol E Sifilogr* 2017; **152**:537–40.

7 Fernández-Figueras MT, Carrato C, Sáenz X, *et al.* Actinic keratosis with atypical basal cells (AK I) is the most common lesion associated with invasive squamous cell carcinoma of the skin. *J Eur Acad Dermatol Venereol* 2015; **29**:991–7.

8 Röwert-Huber J, Patel MJ, Forschner T, *et al.* Actinic keratosis is an early in situ squamous cell carcinoma: a proposal for reclassification. *Br J Dermatol* 2007; **156 Suppl 3**:8–12.

9 Stratigos AJ, Garbe C, Dessinioti C, *et al.* European interdisciplinary guideline on invasive squamous cell carcinoma of the skin: Part 2. Treatment. *Eur J Cancer Oxf Engl 1990* 2020; **128**:83–102.

10 Morton CA, Szeimies R-M, Basset-Seguin N, *et al.* European Dermatology Forum guidelines on topical photodynamic therapy 2019 Part 1: treatment delivery and established indications - actinic keratoses, Bowen's disease and basal cell carcinomas. *J Eur Acad Dermatol Venereol JEADV* 2019; **33**:2225–38.

11 Heppt MV, Leiter U, Steeb T, *et al.* S3 guideline for actinic keratosis and cutaneous squamous cell carcinoma – short version, part 1: diagnosis, interventions for actinic keratoses, care structures and quality-of-care indicators. *JDDG J Dtsch Dermatol Ges* 2020; **18**:275–94.

12 Dejonckheere G, Suppa M, Marmol V del, *et al.* The actinic dysplasia syndrome – diagnostic approaches defining a new concept in field carcinogenesis with multiple cSCC. *J Eur Acad Dermatol Venereol* 2019; **33**:16–20.

13 Zalaudek I, Argenziano G. Dermoscopy of actinic keratosis, intraepidermal carcinoma and squamous cell carcinoma. *Curr Probl Dermatol* 2015; **46**:70–6.

14 Zalaudek I, Giacomel J, Schmid K, *et al.* Dermatoscopy of facial actinic keratosis, intraepidermal carcinoma, and invasive squamous cell carcinoma: a progression model. *J Am Acad Dermatol* 2012; **66**:589–97.

15 Zalaudek I, Giacomel J, Argenziano G, *et al.* Dermoscopy of facial nonpigmented actinic keratosis. *Br J Dermatol* 2006; **155**:951–6.

16 Cinotti E, Labeille B, Debarbieux S, *et al.* Dermoscopy vs. reflectance confocal microscopy for the diagnosis of lentigo maligna. *J Eur Acad Dermatol Venereol JEADV* 2018. doi:10.1111/jdv.14791.

17 Dinnes J, Deeks JJ, Chuchu N, *et al.* Reflectance confocal microscopy for diagnosing keratinocyte skin cancers in adults. *Cochrane Database Syst Rev* 2018; **12**:CD013191.

18 Ferrante di Ruffano L, Dinnes J, Deeks JJ, *et al.* Optical coherence tomography for diagnosing skin cancer in adults. *Cochrane Database Syst Rev* 2018; **12**:CD013189.

19 Valdés-Morales KL, Peralta-Pedrero ML, Cruz FJ-S, Morales-Sánchez MA. Diagnostic Accuracy of Dermoscopy of Actinic Keratosis: A Systematic Review. *Dermatol Pract Concept* 2020; **10**. doi:10.5826/dpc.1004a121.

20 Casari A, Chester J, Pellacani G. Actinic Keratosis and Non-Invasive Diagnostic Techniques: An Update. *Biomedicines* 2018; **6**. doi:10.3390/biomedicines6010008.

21 Jl P, L T, C H, *et al.* Aspect en microscopie confocale par réflectance in vivo des kératoses actiniques: Reflectance confocal microscopy features of actinic keratoses [WWW Document]. Ann. Dermatol. Venereol. 2019; **146 Suppl 2**. doi:10.1016/S0151-9638(19)30201-7.

22 Boone M a. LM, Marneffe A, Suppa M, *et al.* High-definition optical coherence tomography algorithm for the discrimination of actinic keratosis from normal skin and from squamous cell carcinoma. *J Eur Acad Dermatol Venereol JEADV* 2015. doi:10.1111/jdv.12954.

23 Marneffe A, Suppa M, Miyamoto M, *et al.* Validation of a diagnostic algorithm for the discrimination of actinic keratosis from normal skin and squamous cell carcinoma by means of high-definition optical coherence tomography. *Exp Dermatol* 2016; **25**:684–7.

24 Boone M a. LM, Suppa M, Marneffe A, *et al.* A new algorithm for the discrimination of actinic keratosis from normal skin and squamous cell carcinoma based on in vivo analysis of optical properties by high-definition optical coherence tomography. *J Eur Acad Dermatol Venereol JEADV* 2016; **30**:1714–25.

25 Cinotti E, Labeille B, Douchet C, *et al.* Dermoscopy, reflectance confocal microscopy, and high-definition optical coherence tomography in the diagnosis of generalized argyria. *J Am Acad Dermatol* 2017; **76**:S66–8.

26 Dubois A, Levecq O, Azimani H, *et al.* Line-field confocal optical coherence tomography for high-resolution noninvasive imaging of skin tumors. *J Biomed Opt* 2018; **23**:1.

27 Monnier J, Tognetti L, Miyamoto M, *et al.* In vivo characterization of healthy human skin with a novel, non-invasive imaging technique: line-field confocal optical coherence tomography. *J Eur Acad Dermatol Venereol JEADV* 2020; **34**:2914–21.

28 Tognetti L, Cinotti E, Suppa M, *et al.* Line field confocal optical coherence tomography: An adjunctive tool in the diagnosis of autoimmune bullous diseases. *J Biophotonics* 2021; :e202000449.

29 Suppa M, Fontaine M, Dejonckheere G, *et al.* Line-field confocal optical coherence tomography of basal cell carcinoma: A descriptive study. *J Eur Acad Dermatol Venereol JEADV* 2020. doi:10.1111/jdv.17078.

30 Lenoir C, Perez-Anker J, Diet G, *et al.* Line-field confocal optical coherence tomography of benign dermal melanocytic proliferations: a case series. *J Eur Acad Dermatol Venereol JEADV* 2021. doi:10.1111/jdv.17180.

31 Ruini C, Schuh S, Sattler E, Welzel J. Line-field confocal optical coherence tomography-Practical applications in dermatology and comparison with established

imaging methods. *Skin Res Technol Off J Int Soc Bioeng Skin ISBS Int Soc Digit Imaging Skin ISDIS Int Soc Skin Imaging ISSI* 2020. doi:10.1111/srt.12949.

32 Tognetti L, Carraro A, Lamberti A, *et al.* Kaposi sarcoma of the glans: New findings by line field confocal optical coherence tomography examination. *Skin Res Technol Off J Int Soc Bioeng Skin ISBS Int Soc Digit Imaging Skin ISDIS Int Soc Skin Imaging ISSI* 2020. doi:10.1111/srt.12938.

33 Lacarrubba F, Verzì AE, Puglisi DF, Micali G. Line-field confocal optical coherence tomography: a novel, non-invasive imaging technique for a rapid, in-vivo diagnosis of herpes infection of the skin. *J Eur Acad Dermatol Venereol JEADV* 2021. doi:10.1111/jdv.17182.

34 Ruini C, Schuh S, Hartmann D, *et al.* Noninvasive real-time imaging of mite skin infestations with line-field confocal optical coherence tomography. *Br J Dermatol* 2021; **184**:e3.

35 Tognetti L, Rizzo A, Fiorani D, *et al.* New findings in non-invasive imaging of aquagenic keratoderma: Line-field optical coherence tomography, dermoscopy and reflectance confocal microscopy. *Skin Res Technol Off J Int Soc Bioeng Skin ISBS Int Soc Digit Imaging Skin ISDIS Int Soc Skin Imaging ISSI* 2020. doi:10.1111/srt.12882.

36 Tognetti L, Fiorani D, Cinotti E, Rubegni P. Tridimensional skin imaging in aquagenic keratoderma: virtual histology by line-field confocal optical coherence tomography. *Int J Dermatol* 2021; **60**:e52–4.

37 Tognetti L, Fiorani D, Suppa M, *et al.* Examination of circumscribed palmar hypokeratosis with line-field confocal optical coherence tomography: Dermoscopic, ultrasonographic and histopathologic correlates. *Indian J Dermatol Venereol Leprol* 2020; **86**:206–8.

38 Xiang W, Peng J, Song X, *et al.* Analysis of debrided and non-debrided invasive squamous cell carcinoma skin lesions by in vivo reflectance confocal microscopy before and after therapy. *Lasers Med Sci* 2017; **32**:211–9.

39 Schmitz L, Gambichler T, Gupta G, *et al.* Actinic keratoses show variable histological basal growth patterns - a proposed classification adjustment. *J Eur Acad Dermatol Venereol JEADV* 2018; **32**:745–51.

40 Boone M a. LM, Suppa M, Pellacani G, *et al.* High-definition optical coherence tomography algorithm for discrimination of basal cell carcinoma from clinical BCC imitators and differentiation between common subtypes. *J Eur Acad Dermatol Venereol JEADV* 2015. doi:10.1111/jdv.13003.

LEGEND FOR FIGURES

Figure 1. Actinic keratosis: dermoscopic (a), histopathological (b), and line-field confocal optical coherence tomography (LC-OCT) images (c,d). Histopathological examination shows mild keratinocyte atypia in the epidermis and prominent hair follicles (b, white star). LC-OCT examination reveals the presence of atypical keratinocyte nuclei inside the epidermis (red asterisk) and a well outlined dermal-epidermal junction (DEJ, red arrow). A hair follicle is present (c, white star). Scale bar=100 µm.

Figure 2. Actinic keratosis: dermoscopic (a), histopathological (b), and line-field confocal optical coherence tomography (LC-OCT) images (c). LC-OCT examination reveals the presence of hyperkeratosis (white brace), acanthosis (yellow brace) and atypical nuclei of keratinocytes inside the epidermis (red asterisk). The dermal-epidermal junction is not visible. Roundish hyporeflective areas corresponding to glomerular vessels are discernable (white arrow). Scale bar=100 µm.

Figure 3. Squamous cell carcinoma in situ (Bowen subtype): dermoscopic (a), histopathological (b,e), and line-field confocal optical coherence tomography (LC-OCT) images (c,d). LC-OCT examination reveals the presence of hyperkeratosis (white brace), acanthosis (yellow brace), atypical nuclei of keratinocytes inside the epidermis (red asterisk) and roundish hyporeflective areas corresponding to glomerular vessels (white arrow). The dermal-epidermal junction is not visible. An erosion with an overlying crust (d, blue asterisk) is detectable and correlates with histological image (e). Scale bar=100 µm.

Figure 4. Squamous cell carcinoma in situ (Bowen subtype): dermoscopic (a), histopathological (b), and line-field confocal optical coherence tomography (LC-OCT) images (c). LC-OCT examination reveals the presence hyperkeratosis (white brace), acanthosis (yellow brace), and atypical keratinocyte nuclei irregular in size and shape inside the epidermis (red asterisk). The dermal-epidermal junction is visible (red arrow). Roundish hyporeflective areas corresponding to glomerular (white arrow) and linear (light blue) vessels are discernable. Scale bar=100 µm.

Figure 5. Microinvasive squamous cell carcinoma: dermoscopic (a), histopathological (b), and line-field confocal optical coherence tomography (LC-OCT) images (c). LC-OCT examination reveals the presence of hyperkeratosis (white brace), acanthosis (yellow brace), atypical nuclei of keratinocyte (red asterisk) and tumour budding (white arrow). Adnexal involvement is present (yellow star). The dermal-epidermal junction is well outlined (red arrow), except in focal areas (green asterisk). Scale bar=100 µm.

Figure 6. Invasive squamous cell carcinoma: dermoscopic (a), histopathological (b), and line-field confocal optical coherence tomography (LC-OCT) images (c). LC-OCT examination reveals the presence of atypical keratinocyte nuclei irregular in size and shape inside the epidermis (red asterisk). The dermal-epidermal junction is not well outlined (green asterisk) and tumour broad strands (yellow asterisk) are visible. Scale bar=100 µm.

TABLES

Table 1. Description of LC-OCT criteria for actinic keratosis and squamous cell carcinoma (based on literature review and expert opinion)

LC-OCT criteria	Definition
Hyperkeratosis	Stratum corneum thicker than 20 µm
Parakeratosis	Small dark areas corresponding to cell nuclei inside the stratum corneum
Erosion, ulceration	Dark areas with sharp borders and irregular contours filled with amorphous material, cellular debris, and small particles

Acanthosis	Epidermis thicker than 60 µm
Disarranged epidermal architecture	Variation in shape and size of epidermal nuclei of keratinocytes and variation in reflectivity of keratinocytes; the normal architecture of the epidermis with its well-defined different layers is no longer visible
Dyskeratotic keratinocytes	Large hyperreflective round cells inside the epidermis
Atypical nuclei	Irregular in shape and size nuclei
Crowded nuclei	High density of keratinocyte nuclei
Mottled pigmentation of keratinocytes	Presence of clustered hyperreflective keratinocytes
Pigmentation of the basal layer	Hyperreflective basal layer of the epidermis
Keratin pearls	Whorl-shaped accumulation of keratin, appearing as a dark area with hyperreflective and undulated lines
Whorled appearance	Whorled arrangement of keratinocyte nuclei inside the epidermis
Dermal-epidermal junction	Well-defined homogenous hyporeflective small band that separates the epidermis from the dermis. It can be linear or jagged. It was defined as *outlined* when it was not interrupted by tumour proliferations
Adnexal involvement	Enlarged hair follicle epithelium with irregular in shape and size nuclei
Tumour budding	A rounded projection of a complete disarranged epidermis, composed of blurred outlined atypical keratinocytes
Broad strands	Invasive strands of atypical and dyskeratotic keratinocytes interrupting the dermal-epidermal junction and projected irregularly into the dermis
Dilated linear vessels	Large well defined hyporeflective elongated areas in the dermis characterized by the flowing of blood cells in the LC-OCT video modality
Glomerular vessels	Hyporeflective loosely packed and spiral-shaped blood vessels within the superficial dermis
Elastosis	Hypo-reflective areas in the dermis

Table 2. Demographics and clinical features of the study lesions.

	AK	SCC	p*	In situ SCC	Invasive SCC	p**
	N=50	N=108		N=62	N=46	
Gender						
Female	25 (50.0)	58 (53.7)	0.73	33 (53.2)	25 (54.3)	0.90
Male	25 (50.0)	50 (46.3)		29 (46.8)	21 (45.7)	
Mean age (SD)	70.7 (10.9)	69.3 (13.5)	0.53	69.3 (12.6)	69.5 (14.7)	0.82
Body location						
Head/neck	31 (62.0)	59 (54.6)	0.82	38 (61.3)	21 (45.7)	0.29
Trunk	6 (12.0)	14 (13.0)		9 (14.5)	5 (10.9)	
Upper limbs	6 (12.0)	16 (14.8)		9 (14.5)	7 (15.2)	
Lower limbs	7 (14.0)	19 (17.6)		6 (9.7)	13 (28.3)	

Data are presented as number (%), unless otherwise stated.

SD, standard deviation.

*p-values refer to the comparison between AK and SCC.

**p-values refer to the comparison between AK, in situ SCC and invasive SCC

Table 3 Distribution of LC-OCT criteria across study lesions

	AK	SCC	p*	In situ SCC excluding BD	BD	p**	In situ SCC	Invasive SCC	p***
	N=50	N=108		N=37	N=25		N=62	N=46	
Good image quality	38 (76.0)	79 (73.1)	0.85	27 (73.0)	18 (72.0)	1.00	45 (72.6)	34 (73.9)	0.99
Epidermis visualization	47 (95.9)	95 (88.8)	0.23	35 (94.6)	21 (87.5)	0.39	56 (91.8)	39 (84.8)	0.18
Thickness of the lesion excluding SC(µm)									
Minimum (SD)	69 (41)	106 (49)	**<0.001**	107 (48)	93 (44)	0.36	102 (46)	113 (52)	**<0.001**[a,b]
Maximum visible (SD)	153 (71)	214 (53)	**<0.001**	214 (62)	206 (58)	0.603	211 (60)	217 (42)	**<0.001**[a,b]
Mean (SD)	105 (50)	150 (49)	**<0.001**	152 (50)	141 (46)	0.486	148 (49)	154 (49)	**<0.001**[a,b]
Thickness of SC (µm)									
Minimum (SD)	18 (12)	24 (20)	0.06	23 (20)	21 (11)	0.747	22 (17)	27 (23)	0.07
Maximum visible (SD)	96 (94)	103 (89)	0.25	99 (95)	84 (44)	0.407	94 (80)	116 (99)	0.39
Mean (SD)	38 (33)	54 (60)	**0.02**	50 (65)	52 (58)	0.917	51 (62)	57 (58)	**0.04**[b]
Hyperkeratosis	24 (48.0)	77 (71.3)	**0.01**	24 (64.9)	19 (76.0)	0.40	43 (69.4)	34 (73.9)	**0.02**[a,b]
Parakeratosis	20 (64.5)	52 (62.7)	0.85	17 (65.4)	12 (60.0)	0.76	29 (63.0)	23 (62.2)	0.98
Erosion, ulceration	30 (61.2)	66 (62.9)	0.86	24 (68.6)	13 (56.5)	0.40	37 (61.7)	29 (64.4)	0.94
Acanthosis	38 (76.0)	77 (71.3)	0.57	31 (83.8)	16 (64.0)	0.13	47 (75.8)	30 (65.2)	0.44
Disarranged epidermal architecture	35 (77.8)	95 (94.0)	**0.01**	33 (94.3)	22 (91.7)	0.57	55 (93.2)	40 (95.2)	**0.02**[a,b]
Dyskeratotic keratinocytes	37 (82.2)	73 (72.3)	0.22	30 (83.3)	14 (58.3)	**0.04**	44 (73.3)	29 (70.7)	0.41
Visible nuclei	48 (96.0)	102 (95.3)	0.99	36 (97.3)	24 (96.0)	1.00	60 (96.8)	42 (93.3)	0.86
Atypical nuclei	41 (87.2)	94 (91.3)	0.56	31 (86.1)	22 (91.7)	0.69	53 (88.3)	41 (95.3)	0.38
Crowded nuclei	23 (50.0)	47 (47.0)	0.86	16 (44.4)	13 (56.5)	0.42	29 (49.2)	18 (43.9)	0.83
Features of epidermal dysplasia	42 (84.0)	99 (91.7)	0.17	34 (91.9)	23 (92.0)	1.00	57 (91.9)	42 (91.3)	0.4
Whorled appearance	0	2 (2.0)	0.99	0 (0.0)	2 (8.3)	0.17	2 (3.4)	0	0.34
Visible DEJ	24 (48.0)	44 (40.7)	0.40	17 (45.9)	10 (40.0)	0.79	27 (43.5)	17(37.0)	0.56
Outlined DEJ	23 (46.0)	22 (20.4)	**0.01**	13 (35.1)	6 (24.0)	0.41	19 (30.7)	3(6.5)	**<0.001**[b,c]
Adnexal involvement	21 (47.7)	31 (36.5)	0.26	13 (40.6)	8 (40.0)	1.00	21 (40.4)	10 (30.3)	0.30
Tumour budding	19 (45.2)	31 (40.8)	0.7	11 (39.3)	5 (33.3)	0.75	16 (37.2)	15 (45.5)	0.7
Broad strands	1 (3.2)	26 (38.8)	**<0.001**	0 (0.0)	3 (25.0)	0.05	3 (9.7)	23 (63.9)	**<0.001**[b,c]
Dilated linear vessels	35 (77.8)	53 (56.4)	**0.02**	21 (61.8)	11 (50.0)	0.41	32 (57.1)	21 (55.3)	0.05
Glomerular vessels	37 (78.7)	61 (66.3)	0.17	24 (70.6)	13 (61.9)	0.56	37 (67.3)	24 (64.9)	0.30

Elastosis	11 (26.2)	9 (12.3)	0.08	5 (19.2)	2 (10.0)	0.45	7 (15.2)	2 (7.4)	0.12

Data are presented as number (%) unless otherwise stated.

Percentages are calculated on the total of the evaluable cases: numbers do not always add up to the total of AKs and SCCs due to missing values (criteria were not evaluated in case of poor image quality and/or focal visualization of the corresponding skin layer).

*p-values refer to the comparison between AK and SCC.

**p-values refer to the comparison between BD and SCC in situ excluding BD.

***p-values refer to the comparison between AK, in situ SCC (including BD) and invasive SCC: statistically significant are reported for the comparison between AK and in situ SCC (a), between AK and invasive SCC (b), and between in situ SCC and invasive SCC (c).

Lesions were considered as having features of epidermal dysplasia if at least one criterion among disarranged epidermal architecture, dyskeratotic keratinocytes, and atypical nuclei was found.

AK, actinic keratosis; BD, Bowen's disease; SC, stratum corneum; SCC, squamous cell carcinoma; SD, standard deviation; DEJ, dermal-epidermal junction.

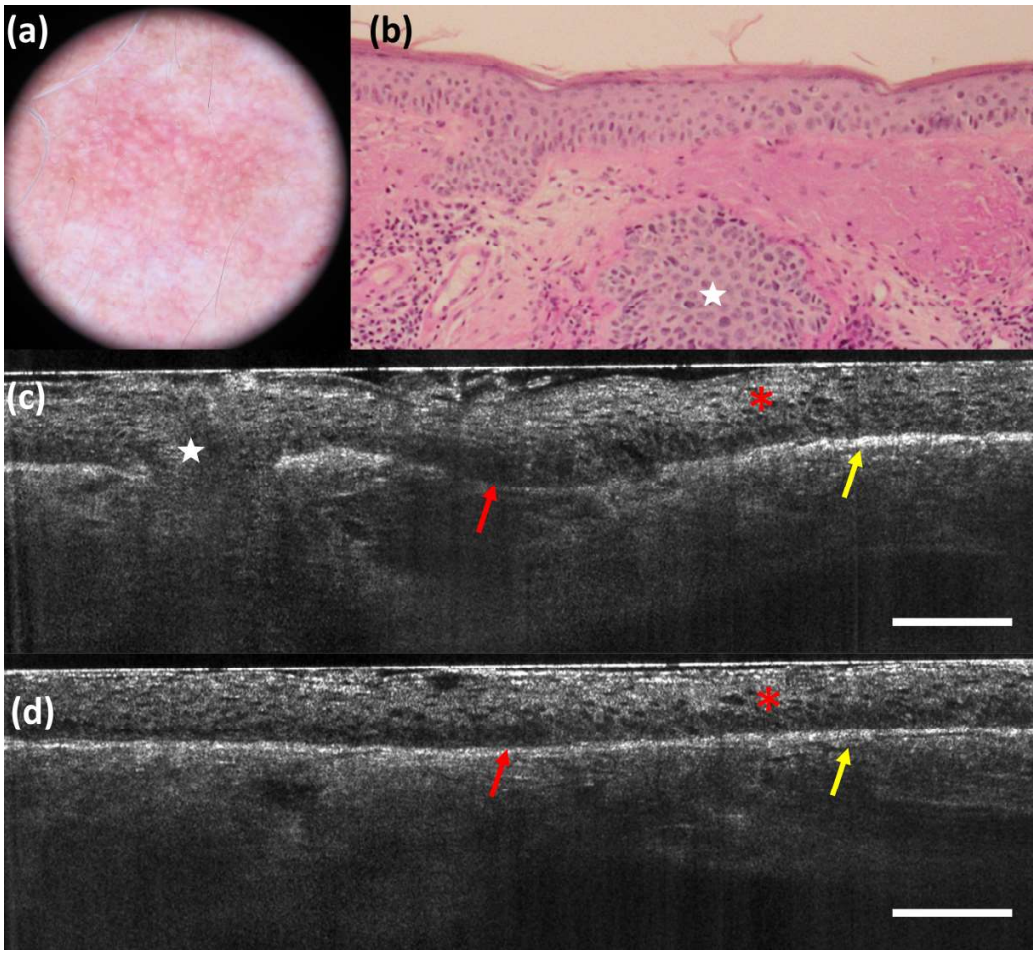

ced_14801_f1.tif

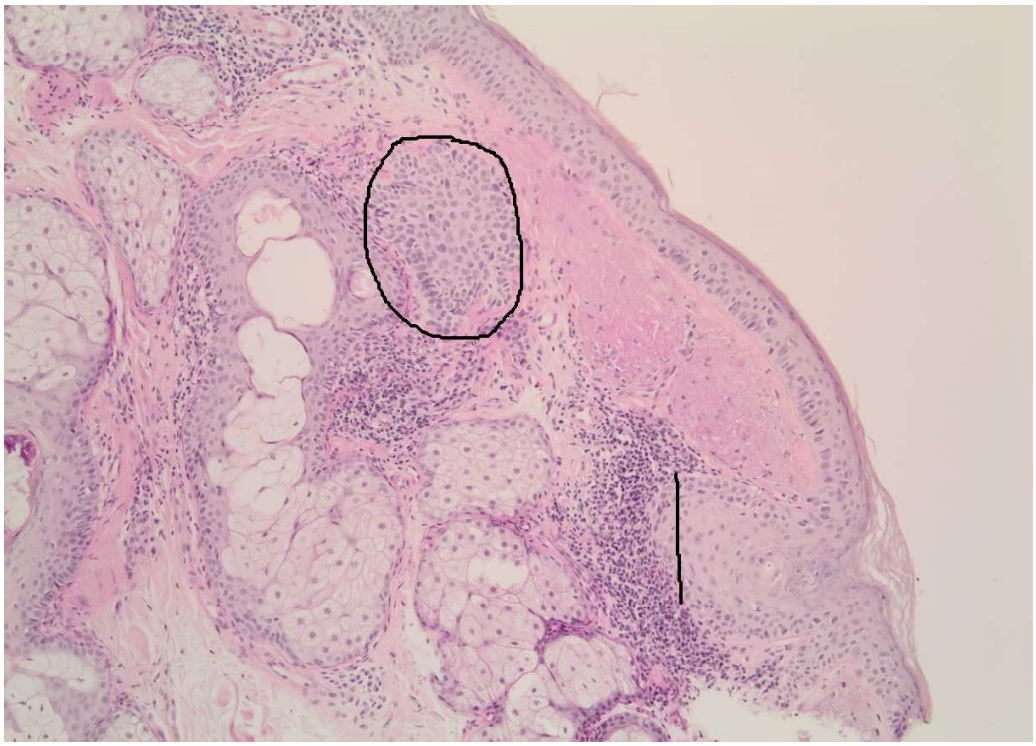

ced_14801_f1b.tif

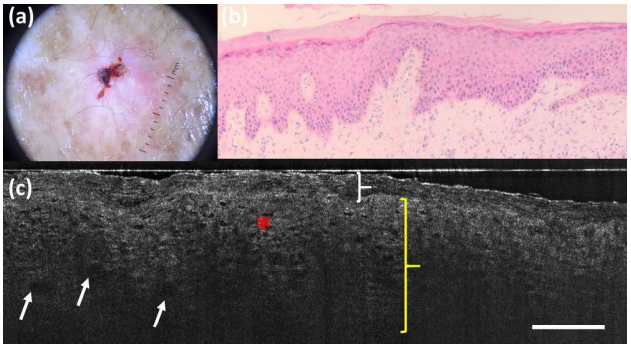

ced_14801_f2.tif

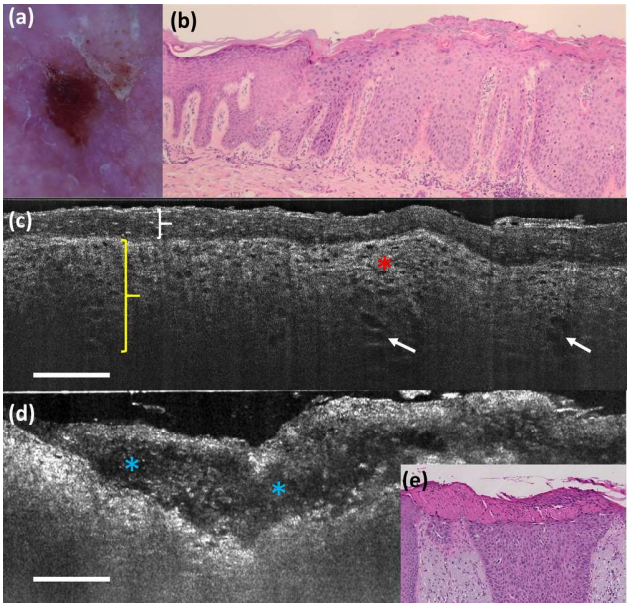

ced_14801_f3.tif

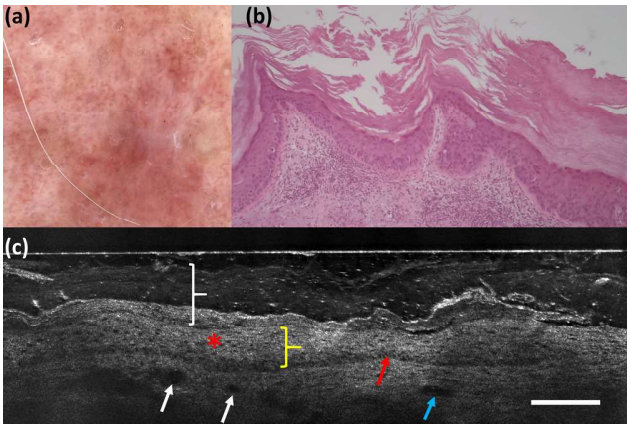

ced_14801_f4.tif

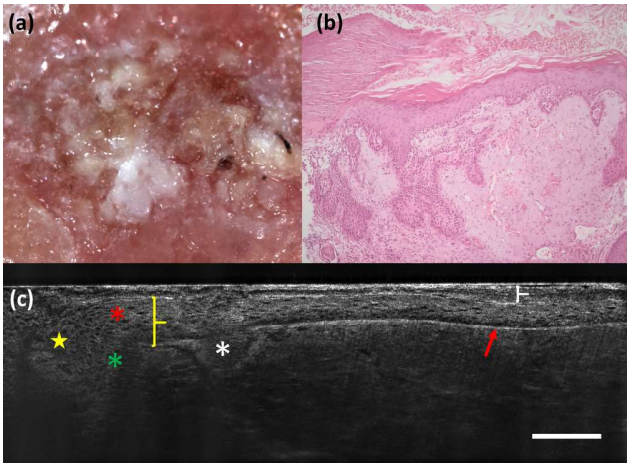

ced_14801_f5.tif

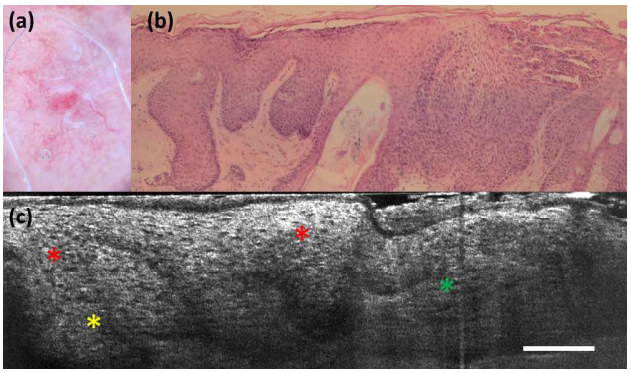

ced_14801_f6.tif